16th World Congress in Computational Mechanics (WCCM)
21-26 July 2024, Vancouver, Canada
A. Korobenko, M. Laforest, S. Prudhomme, R. Vaziri (Eds)

NUMERICAL STUDIES OF COMPRESSION FAILURE IN TRIPLY PERIODIC MINIMAL SURFACE-BASED CERAMIC STRUCTURES

THI NGOC DIEP TRAN*[1], ROMANA PIAT*[2]

* Faculty of Math. & Nat. Sciences, Darmstadt University of Applied Sciences
Schöfferstraße 3, 64295 Darmstadt, Germany
[1] thi-ngoc-diep.tran@h-da.de

[2] romana.piat@h-da.de

Key words: triply periodic minimal surface, porous structures, finite element analysis, crack propagation, damage development, compression failure

Abstract. Microstructures with minimal surfaces can be often found in natural porous architectures, where the surface tension minimizes the area. The triply periodic minimal surfaces (TPMS) [1] are an example of such microstructures. Compared with other porous structures, TPMS have three significant features: firstly, their geometries can be completely expressed via analytical functions; secondly, TPMS are periodic in three independent directions and thirdly, the mean curvature of TPMS is zero [2]. Transforming the TPMS-based unit cell into a lattice structure has particular usage in aerospace, nuclear energy, and biomedical applications where light weight, high stiffness, and temperature resistance are of critical importance. In the presented studies, the failure behavior of four typical TPMS structures (Primitive, Gyroid, Neovius, and IWP) under compression was studied using finite element analysis. Numerical modeling of the damage propagation and strength prediction was performed by removing the finite elements in which the appropriate damage criterion is reached. Utilizing the equations of the generated TPMS structures, the wall thickness of unit cell was considered the main parameter that defined the ceramics volume fraction and should be taken into consideration. Therefore, various unit cell models for different wall thicknesses were generated and used to investigate the impact of the cell geometry on the damage initiation, propagation, and overall compression strength. The results of compression strength and damage development were compared with those of other TPMS structures for the same wall thickness and volume fraction. Finally, the grade TPMS porous structure was provided to verify the effect of wall thickness variation on damage evolution on the macroscale.

1 INTRODUCTION

Inspired by the porous structures in nature such as bone, wood, and honeycombs, artificial porous materials are manufactured and applied in wide-ranging engineering applications. Certain patterns observed in butterfly wings and weevil exoskeletons closely resemble TPMS structures, which implies the bionic applications potential of TPMS [2, 3]. Based on the degree of control over geometric features, the design methods of porous structures can be classified into three types [4]. The first type of porous structure is the three-dimensional foam, which can

be generated by stochastically introducing voids in the bulk of solid material e.g., through salt leaching or gas-foaming [5, 6]. Thus, controlling the porous characteristics and performances of foam is complicated. The second type of porous structure is lattice structure, which has unit cells constructed from a network of struts connected at nodes. The shapes and features of lattice structures can be easily regulated by modifying the length and radius of the struts, as well as adjusting the topology of strut connections. The third type of porous structure is designed by the triply periodic minimal surface (TPMS), where the whole structure can be expressed by mathematical functions and directly controlled by adjusting the function parameters [1].

It has been shown in [7], that cellular structures exhibit consistently specific properties compared to their bulk material counterparts, e.g., for application to electronic displays. A glass substrate is layered with a thin film in a gyroid structure. By filling the lattice with suitable electrolytes, the device can function as an electrochromic device. This gyroid thin film can endure a significant temperature excursion and swelling strain without causing yield, in contrast to a solid film of the same material. These TPMS-based structures are characterized by their minimal area properties, which means the average curvature at every point among the surfaces with the same boundary is zero [8]. Different from lattice-based structures, TPMS does not consist of nodes and struts, where imperfections in joints within the lattice can lead to deterioration in both elastic and plastic properties [7]. Therefore TPMS-based structures can provide notable manufacturing advantages by their highly interconnected architectures and improve the overall properties. Despite being from the same family, these individual structures (Gyroid, Primitive, IWP, and Neovius) may demonstrate varying performances. For various types of TPMS structures, periodic and unit cell analysis with different wall thicknesses are performed in this study using the Finite Element (FE) software (ABAQUS) [9] to investigate the compression failure behavior, including damage initiation, damage propagation, and overall compression strength.

2 MODELLING METHODS

In this section, the method to generate the TPMS microstructures and numerical studies to control their structure are provided. For this purpose, different approaches and software were used. In the preliminary work, four typical TPMS-based cell structures (Gyroid, Primitive, IWP, and Neovius) are considered and presented as architected sheets. When generating the periodic repetition of TPMS, it is distinguished between uniform and graded porous structures. All the cellular structures of uniform TPMS have the same size and wall thickness, while the graded TPMS-based geometry incorporates variations in curvature and wall thickness.

2.1 Uniform TPMS

As mentioned before, the whole geometry of TPMS can be completely generated via mathematical equations. TPMS is classified as an implicit surface, which can be described as $f(x, y, z) = C$ as follows:

Gyroid:

$$f(x,y,z) = \sin(\omega_y y)\cos(\omega_x x) + \sin(\omega_z z)\cos(\omega_y y) + \sin(\omega_x x)\cos(\omega_z z) = C \quad (1)$$

Primitive:

$$f(x,y,z) = \cos(\omega_x x) + \cos(\omega_y y) + \cos(\omega_z z) = C \quad (2)$$

IWP:

$$f(x,y,z) = 2[\cos(\omega_x x)\cos(\omega_y y) + \cos(\omega_y y)\cos(\omega_z z) + \cos(\omega_z z)\cos(\omega_x x)] - [\cos(2\omega_x x) + \cos(2\omega_y y) + \cos(2\omega_z z)] = C \quad (3)$$

Neovius:

$$f(x,y,z) = 3[\cos(\omega_x x) + \cos(\omega_y y) + \cos(\omega_z z)] + 4\cos(\omega_x x)\cos(\omega_y y)\cos(\omega_z z) = C, \quad (4)$$

where ω denotes the period and C determines the expansion of the surface in three dimensions. According to the parameter C, space is divided into two intertwined parts by the minimal surface without wall thickness as $f(x,y,z) = C > 0$ and $f(x,y,z) = C < 0$. The TPMS-based unit cells and their 2x2x2 periodic repetition in space are generated using MATLAB [10] and shown in Figure 1.

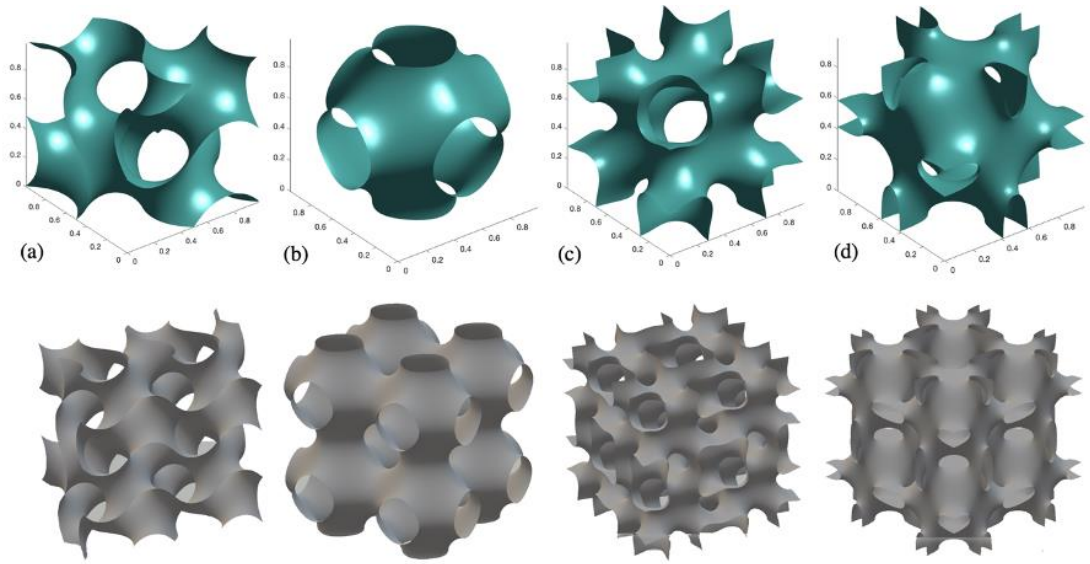

Figure 1: Unit cells and periodic repetition without wall thickness of a) Gyroid b) Primitive c) IWP d) Neovius

To create a TPMS-based object for additive manufacturing and further numerical investigation, the surface structure needs to be converted into a solid. This work focuses on constructing sheet solid objects, which can be generated by shifting the non-thickness surfaces in opposite directions, and the nodes of the two planes are connected in turn. The amount of shift determines the final wall thickness. Hence, a structure with a given wall thickness can be generated using the mathematical function and saved as a stereolithography (STL) file. This STL file is imported into MeshLab [11] to improve the meshing structure. After that, this STL file is processed as a solid body using the freely available software FreeCAD [12] and converted to a STEP file for FE simulations. Figure 2 shows this workflow schematic of a Primitive unit cell when $C = 0.35$ as an example.

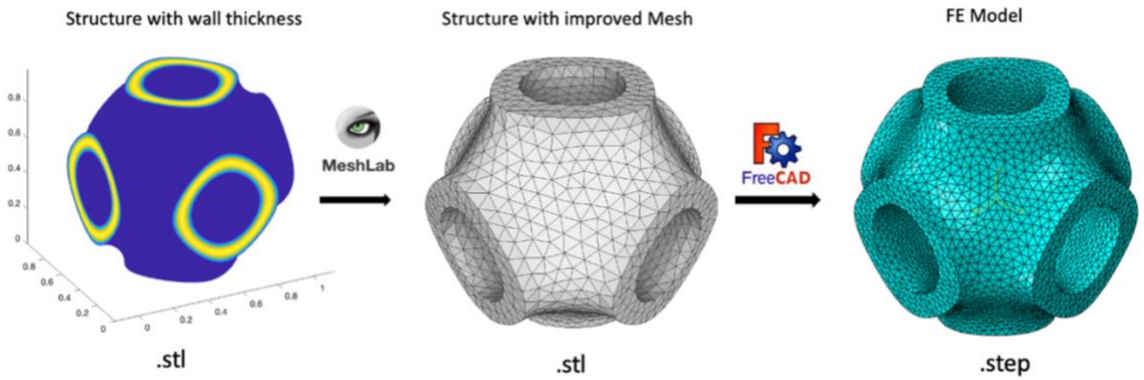

Figure 2: Process to generate a FE model of Primitive unit cell

2.1 Graded TPMS

Although TPMS-based materials have significant potential due to their unique topological properties, their uniform structural design may exhibit limitations under complex conditions. Graded porous structures are found widely in nature and have been proven to be highly mechanically efficient in applications across various engineering fields while maintaining their lightweightness [13-15]. For example, the internal structure of bone tissue transforms gradually from compact in the outer layer to spongy in the interior. Hence, the realization of artificial materials with graded porous architectures represents a compelling method for achieving similar performance observed in natural architecture.

In this work, the graded TPMS is visualized and generated using the developed design Software MD-TPMS [16]. The gradient can be defined through the matrix, e.g. using a 1D matrix (1D array) can control the structure along the Z-axis, and a 2D matrix can control the gradient distribution across the X-Z plane. By utilizing the interpolation resampling algorithm, the user-defined matrix can be seamlessly adjusted. This allows for the incorporation of gradients without introducing discontinuous transitions in the final surface structure. The graded porous structures of Primitive and IWP using the 1D matrix are shown in Figure 3.

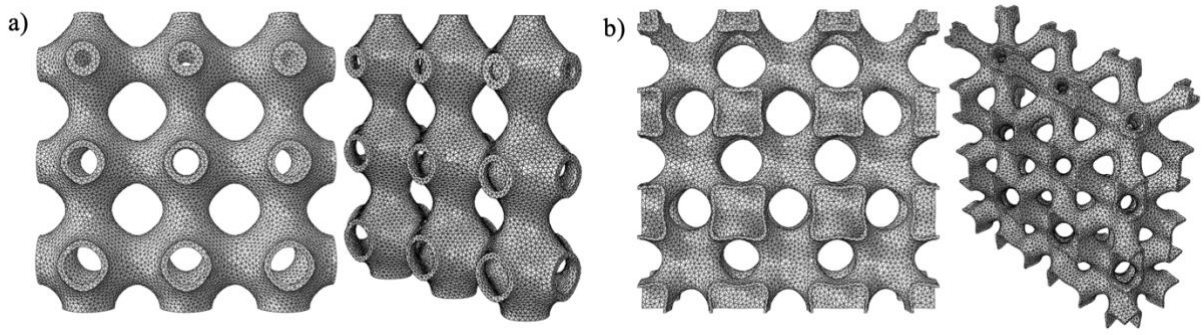

Figure 3: 3D gradient design of a) Primitive b) IWP

3 FINITE ELEMENT MODELING

The mechanical performance of TPMS sheets (Primitive, Gyroid, Neovius, IWP) is investigated computationally using the finite element method. For the parametric study, various 3D models are created to examine the influence of wall thickness as well as volume fraction on compression strength and damage behavior.

3.1 Modeling process

The unit cells of four investigated TPMS structures are used to demonstrate the compression test by applying boundary conditions for uniaxial loading. In this work, the periodicity of the structure was obtained by constraining the parallel movement of the surfaces using the prescribed displacement boundary conditions adopted as follows:

$$u_2 = \lambda \boldsymbol{e_2}, \tag{5}$$

$$u_{1|I} = u_{1|J}, \forall I, J \in \mathcal{B}_1 \tag{6}$$

$$u_{3|I} = u_{3|J}, \forall I, J \in \mathcal{B}_3, \tag{7}$$

where I, J are the nodes on the same surface, $\boldsymbol{e_i}$ are the unit base vector, and $\mathcal{B}_i$ are the surfaces with the unit normal vector in the i-direction. The accuracy of a finite element model can be improved with mesh refinement. By increasing the mesh element density, the integration points are closer to stress concentration regions and the numerical solution can converge to the correct solution [17]. The first-order tetrahedral element C3D4 with 0.02 as the global seed size was applied for all FE models with approximately 165,000 elements. To simulate a compression test, the TPMS-based cell structure was placed between two rigid plates. The upper plate can only move along the vertical direction meanwhile all degrees of freedom of the bottom plate were fixed. Rough friction was implemented as general contact to ensure no relative motion between the rigid plates and the TPMS structure. For all test simulations, the unit cells were subjected to compressive loading until a 10% strain state was achieved. The FE simulation was conducted using Abaqus Explicit dynamic analysis as shown in Figure 4.

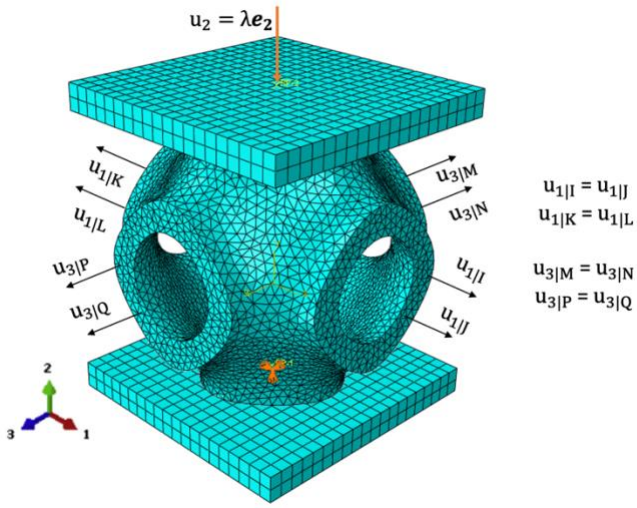

Figure 4: FE model of Primitive unit cell under compression with prescribed displacement boundary conditions

The material parameters for zirconia ceramics used in this work were derived from [18]. The material behavior was described using the Johnson-Cook constitutive model as follows:

$$\sigma = [A + B(\varepsilon)^n][1 + C\ln(\dot{\varepsilon}/\dot{\varepsilon}_0)]\left[1 - \left((T - T_r)/(T_m - T_r)\right)^m\right], \quad (8)$$

where σ is the equivalent stress, $\varepsilon, \dot{\varepsilon}$, $\dot{\varepsilon}_0$ are the equivalent plastic strain, equivalent plastic strain rate, and reference strain rate, respectively. *A, B, C, n,* and *m* are the material constants under reference conditions, denoting yield stress, strain hardening constant, strengthening coefficient of strain rate, strain hardening coefficient, and thermal softening, respectively. *T* is the maximum temperature, T_r is room temperature and T_m is melting temperature of the material. In Abaqus, the damage is described by the progressive reduction of the material stiffness, ultimately leading to failure. The damage in the material was simulated by removing the finite elements when the failure criteria of the model were reached. The Johnson-Cook is a specific ductile damage criterion using equivalent plastic strain $\bar{\varepsilon}_D^{pl}$ to predict damage initiation and is given by [19]:

$$\bar{\varepsilon}_D^{pl} = [d_1 + d_2\exp(-d_3\eta)]\left[1 + d_4\ln\left(\frac{\dot{\bar{\varepsilon}}^{pl}}{\dot{\varepsilon}_0}\right)\right](1 + d_5\hat{T}), \quad (9)$$

where d_1, d_2, d_3, d_4, d_5 are damage variables. The temperature $\hat{T}$ is defined as:

$$\hat{T} \equiv \begin{cases} 0 & \text{, if } T < T_t \\ (T - T_t)/(T_m - T_t), & \text{if } T_t \le T \le T_m, \\ 1 & \text{, if } T > T_m \end{cases} \quad (10)$$

where *T* is the current temperature, T_m is the melting temperature same as in Eq. (8), and T_t is the transition temperature. The material property evaluation should be conducted at or below the transition temperature.

3.2 Model variation

Since the TPMS structures are generated by mathematical equations, variations in the model geometry can be achieved by adjusting the offset wall thickness parameter C. The wall thickness is considered the main variable that affects the volume fraction. Figure 5 shows examples of thickness variation in Primitive and Gyroid unit cells. To analyze the wall thickness influences, various models based on thickness variations for each investigated TPMS structure are presented in Table 1. The value of parameter *C* was assigned differently in each structure to achieve the relative thicknesses ($\boldsymbol{\phi_T}$) between 0.03 and 0.1. Relative thickness refers to the dimensionless ratio between the generated thickness and the overall length of the structure. The ratio of θ between relative thickness (ϕ_T) and volume fraction (ϕ_V) is also incorporated into the analysis. The corresponding values of θ to offset wall thickness parameter *C* are shown in Table 2.

$$\theta = \phi_T/\phi_V. \quad (11)$$

The examination in Table 1 provided four distinct TPMS unit cells with the same volume fraction $\phi_V \approx 0.22$ across varying C values ($C_{Primitive}$ = 0.40, $C_{Gyroid} = 0.35$, $C_{Neovius} = 0.52$, *and* $C_{IWP} = 0.87$). Different TPMS structures with nearly same relative wall thickness $\phi_T \approx 0.08$ were also carried out using $C_{Primitive}$ = 0.30, $C_{Gyroid} = 0.35$, $C_{Neovius} = 0.52$,

and $C_{IWP} = 0.87$. Table 2 reveals that the Primitive unit cells provided significantly larger values of the ratio $\theta \in (0.5;\ 0.56)$ compared to other structures $\theta \in (0.29;\ 0.397)$.

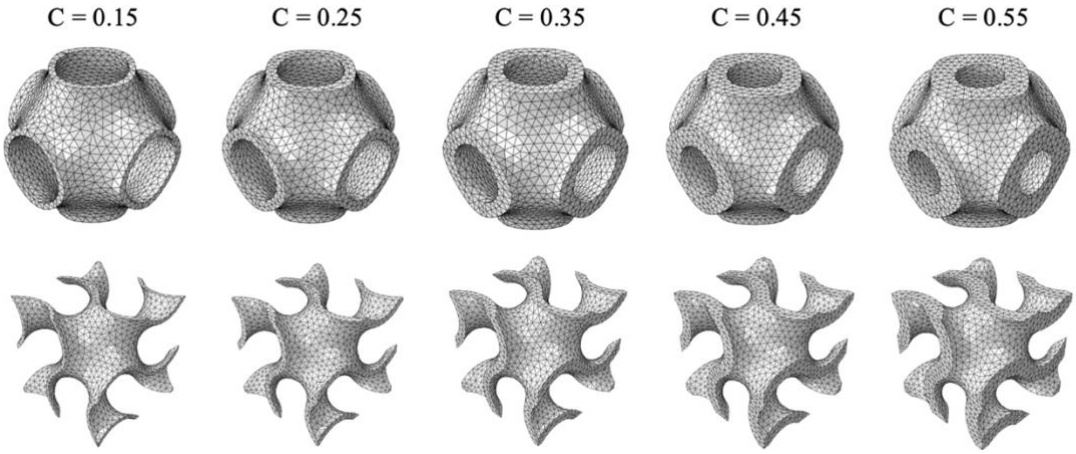

Figure 5: Offset wall thickness parameter variation of Primitive and Gyroid unit cells

Table 1: Corresponding relative thickness and volume fraction to offset wall thickness parameters

Primitve			Gyroid			Neovius			IWP		
C	ϕ_T	ϕ_V	C	ϕ_T	ϕ_V	C	ϕ_T	ϕ_V	C	ϕ_T	ϕ_V
0.15	0.0412	0.0813	0.15	0.0351	0.0905	0.35	0.0529	0.146	0.5	0.0363	0.125
0.25	0.071	0.138	0.25	0.0602	0.155	0.45	0.0711	0.19	0.6	0.0458	0.152
0.30	**0.088**	0.167	0.35	**0.0859**	**0.22**	0.52	**0.0828**	**0.221**	0.7	0.0554	0.179
0.35	0.104	0.195	0.45	0.111	0.284	0.55	0.0899	0.235	0.8	0.0673	0.206
0.40	0.123	**0.223**	0.55	0.138	0.348	0.65	0.110	0.279	0.87	**0.0809**	**0.224**

Table 2: Corresponding ratio θ to offset wall thickness parameters

Primitive		Gyroid		Neovius		IWP	
C	θ	C	θ	C	θ	C	θ
0.15	0.5068	0.15	0.3878	0.35	0.3623	0.5	0.2904
0.25	0.5145	0.25	0.3884	0.45	0.3742	0.6	0.3013
0.30	0.5279	*0.35*	0.3905	*0.52*	0.3746	0.7	0.3095
0.35	0.5333	0.45	0.3908	0.55	0.3825	0.8	0.3267
0.40	0.5516	0.55	0.3966	0.65	0.3958	0.87	0.3612

4 RESULTS AND DISCUSSION

4.1 Compression failure of TPMS unit cells with different wall thicknesses

This section investigates the compressive failure mechanisms of TPMS unit cells with varied wall thicknesses obtained computationally. Figure 6 presents the force-strain curves for four TPMS structures with varying *C* parameters. The point at which cracks begin to form in each structure is also indicated on the graphs by an X mark. All four diagrams consistently demonstrated a proportional correlation between compression strength and the offset wall thickness parameter, namely higher *C* values correspond to higher compression strength. The force-strain curves of Primitive structure exhibited a plateau shape, which signified its enhanced capacity to withstand compressive loads compared to the other structures. Furthermore, no significant difference was observed when crack initiation occurs at different wall thicknesses within the same structure.

Figure 7 compared the force-strain curves of four structures with the same relative thickness and volume fraction obtained from Table 1, allowing for a focused investigation of the inherent properties of each architecture. The analysis revealed a hierarchy in compressive strength, where the IWP structure required the highest compression load for the same amount of displacement, followed by Neovius, Gyroid, and Primitive, respectively. Interestingly, this correlation is related to the ratio θ, namely $\theta_{IWP} = 0.3612 < \theta_{Neovius} = 0.3746 < \theta_{Gyroid} = 0.3905 < \theta_{Primitive} = 0.5279$ (same relative thickness) or $\theta_{Primitive} = 0.5516$ (same volume fraction). Despite its superior compressive strength, the IWP structure appeared susceptible to earlier failure. In contrast, the Primitive structure's characteristic plateau curve indicated its ability to sustain a longer pressure. Crack initiation appeared earliest in the Gyroid structure, followed by Neovius and IWP. The Primitive structure demonstrated the most robust behavior with the latest instance of crack initiation.

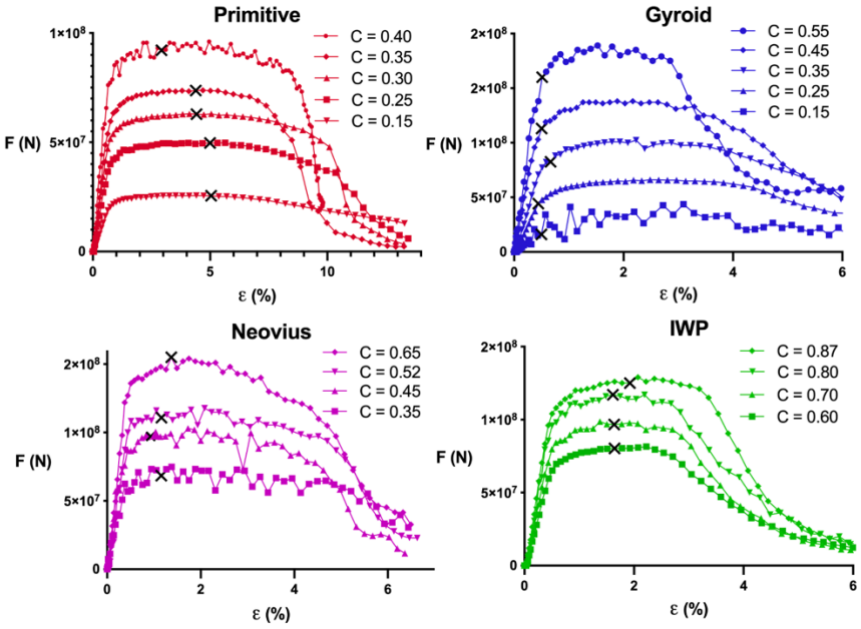

Figure 6: Force-strain curves and indicated first crack of TPMS unit cells at different offset wall thicknesses

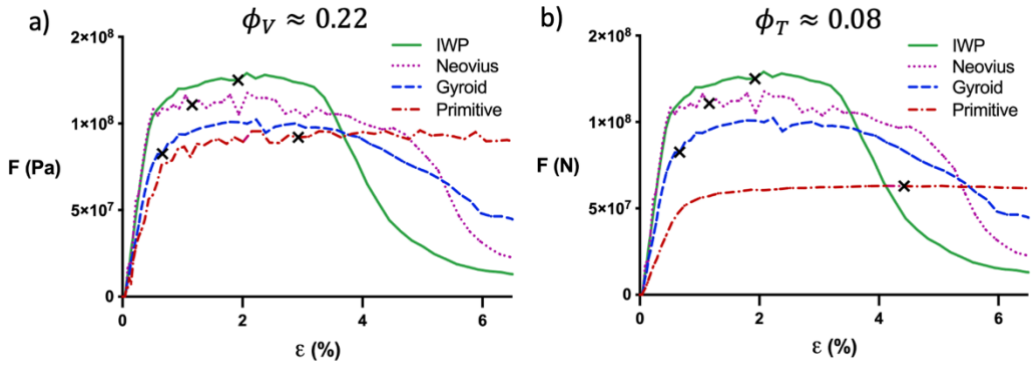

Figure 7: Force-strain curves and indicated first crack of TPMS unit cells at a) same volume fraction b) same relative wall thickness

The corresponding damage development at 4%, 6%, and 8% of compression strain of TPMS unit cells by the same volume fraction is illustrated in Figure 8a. Consistent with the observations in Figure 7a, the damage progression in the Primitive structure demonstrated a remarkable slowdown in the failure process compared to other geometries. While Gyroid, Neovius, and IWP structures achieved an imminent final failure at the compressive strain of 6%, the Primitive structure provided only partially localized cracks at this stage. In all types, the contact region between the structure and the top rigid plate was observed as weak spots, which initiated cracks and then propagated through the entire structure. As a notable outcome, the 3x3x3 periodic repetition of Gyroid structure retained the location of the first deleted finite element as observed in the single Gyroid unit cell as shown in Figure 8b.

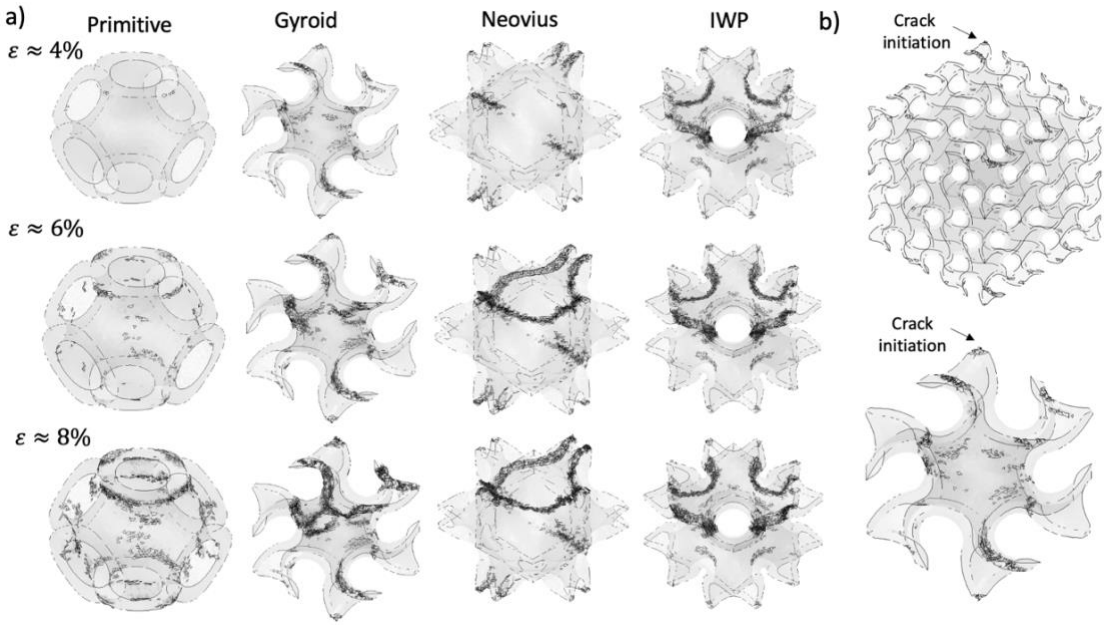

Figure 8: a) Damage development of TPMS unit cells with the same volume fraction b) Comparison of crack development in 3x3x3 Gyroid vs Gyroid unit cells at $\varepsilon \approx 4\%$

4.2 Compression failure of graded TPMS

This section delves into the behavior of graded structures of the Primitive and IWP designs, which represent the extremes of compression strength observed in the previous analysis (Primitive - lowest, IWP - highest). The investigation focuses on 3x1 graded structures generated using a 1D matrix as illustrated in Figure 3. The Primitive structure incorporates graded wall thickness through offset parameters that increase progressively from 0.1 at the bottom layer to 0.4 and to 0.7 at the top layer. The accordingly offset parameters in the IWP structure are 0.5, 1.5, and 2.5. Both graded porous structures (called as $P01-04-07$ and $I05-15-25$) have the same volume fraction $\phi_V = 0.113$. An evaluation is conducted for each graded structure, employing a corresponding uniform structure as a baseline for comparison. This uniform structure maintains the constant wall thickness across three layers extracted from the graded structure. i.e., P01, P04, P07 for Primitive structure, and I05, I15 for IWP structure.

In Figures 9a, the compressive strength of graded TPMS structures landed between the maximum value exhibited by uniform structure with the thickest wall and other structures with thinner walls. However, the graded structure has shown better resistance by its extended plateau region and therefore demonstrated a balance in mechanical performance, surpassing that of uniform counterparts. The graded Primitive and IWP with the same volume fraction exhibited compressive behavior that reflects their unit cells. As observed in Figure 9c, the IWP-based graded structure achieved a higher peak compressive load but more rapid failure. Conversely, the graded Primitive structure exhibited a lower peak load but more resistance.

Figure 10 and Figure 11 have shown distinct crack propagation patterns between the uniform and graded structures. In the IWP structures, cracks predominantly propagated along the horizontal direction (Figure 11). In contrast, cracks within the Primitive graded structures exhibited a more scattered distribution and spread diagonally throughout the structure (Figure 10). The uniform Primitive structure with the thickest walls (P07) displayed a unique behavior, where cracks primarily accumulated on the top surface - the region in direct contact with the rigid plate. As observed, the crack initiation within the Primitive structure preferentially occurred at the intersection regions crossing the unit cells. In the IWP structure, crack formation appeared at weak locations characterized by thin wall thickness across the geometry.

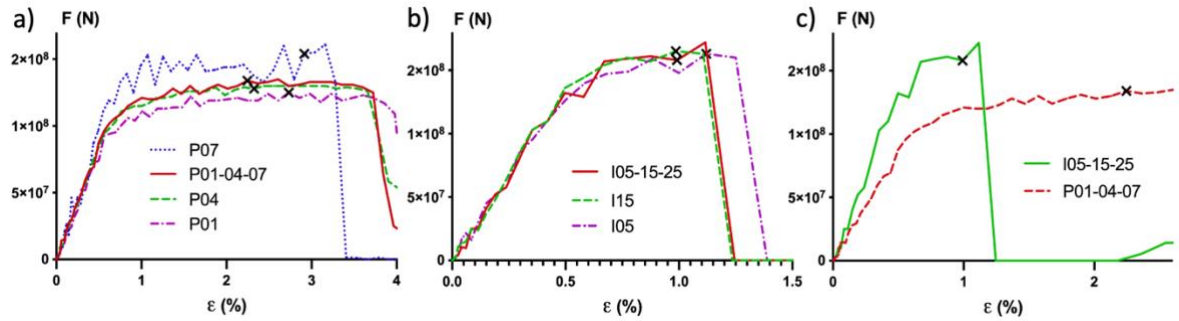

Figure 9: Force-strain curves of uniform and graded a) Primitive b) IWP c) Graded Primitive vs IWP

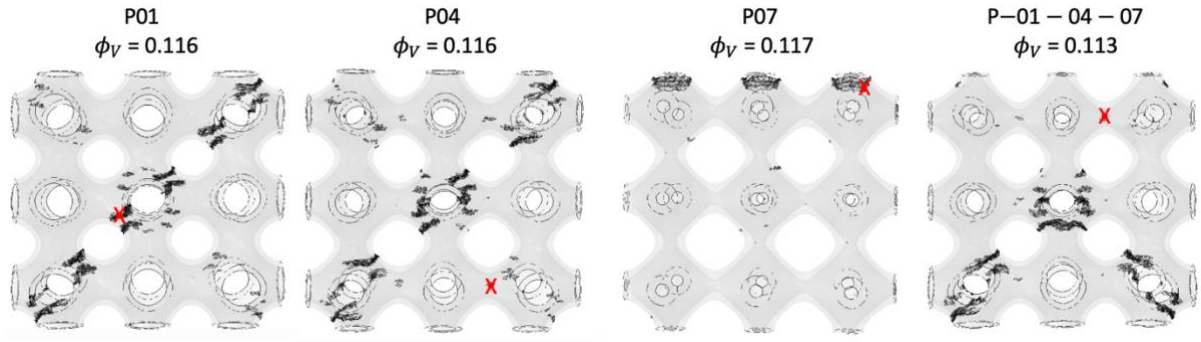

Figure 10: Crack propagation on uniform and graded Primitive structures

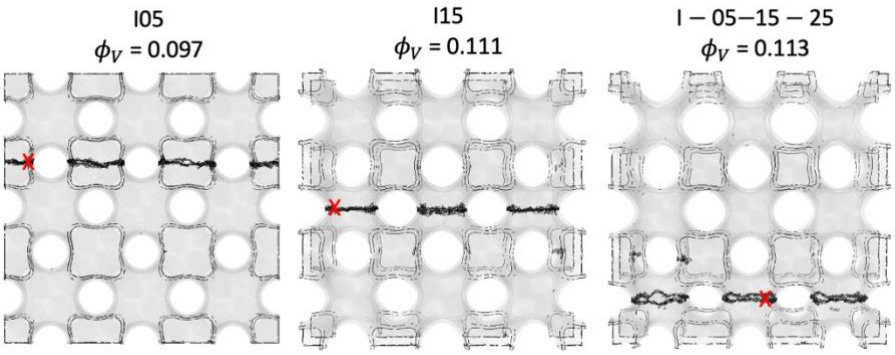

Figure 11: Crack propagation on uniform and graded IWP structures

5 CONCLUSIONS

This study investigated the compressive behavior of four TPMS-based ceramic structures with varying wall thicknesses. The analysis revealed an impact of the ratio θ between the relative thickness and volume fraction to compression strength, with a lower ratio leading to a higher load comparing four different TPMS-based structures. The IWP structure achieved the highest peak load but transitioned rapidly to failure, while the Primitive structure yielded a lower peak load but displayed superior resistance due to its extended damage progression. Furthermore, graded structures mirrored the behavior of their base unit cells, achieving a well-balanced performance compared to uniform counterparts. Crack formation occurred primarily at geometric weaknesses, such as in thin sections or cell transition.

ACKNOWLEDGMENT

The financial support of the University of Applied Sciences Darmstadt and DAAD is gratefully acknowledged.

REFERENCES

[1] Sadeghi, F., Baniassadi, M., Shahidi, A. and Baghani, M. TPMS metamaterial structures based on shape memory polymers: Mechanical, thermal and thermomechanical assessment. *J. Mater. Res. Technol.* (2023) **23**:3726–3743.

[2] Gan, Z., Turner, M. D. and Gu, M. Biomimetic gyroid nanostructures exceeding their natural origins. *Sci. Adv.* (2016) **2**(5):e1600084.
[3] Han, L. and Che, S. An Overview of Materials with Triply Periodic Minimal Surfaces and Related Geometry: From Biological Structures to Self-Assembled Systems. *Adv. Mater*. (2018) **30**(17):1705708.
[4] Feng, J., Fu, J., Yao, X. and He, Y. Triply periodic minimal surface (TPMS) porous structures: from multi-scale design, precise additive manufacturing to multidisciplinary applications. *Int. J. Extreme Manuf.* (2022) **4**:022001.
[5] Ali, H. M. A., Abdi, M. and Sun, Y. Insight into the mechanical properties of 3D printed strut-based lattice structures. *Prog. Addit. Manuf*. (2022) **8**:919–931.
[6] Dehghani, F. and Annabi, N. Engineering porous scaffolds using gas-based techniques. *Curr. Biotechnol.* (2011) **22**:661–666 .
[7] Khaderi, S. N., Deshpande, V. S. and Fleck, N. A. The stiffness and strength of the gyroid lattice. *Int. J. Solids Struct.* (2014) **51**:3866–3877.
[8] Torquato, S. and Donev, A. Minimal surfaces and multifunctionality. *Proc. Math. Phys. Eng. Sci.* (2004) **460**:1849–1856.
[9] Smith, M. ABAQUS/Standard User's Manual, Version 6.9 (2009).
[10] The MathWorks Inc. (2022).
[11] MeshLab (Version 2022.02). https://www.meshlab.net/
[12] FreeCAD (Version 0.20.2). https ://www.freecad.org/
[13] Qureshi, Z. A., Al-Omari, S. A. B., Elnajjar, E., Al-Ketan, O. and Al-Rub, R. A. On the effect of porosity and functional grading of 3D printable triply periodic minimal surface (TPMS) based architected lattices embedded with a phase change material. *Int. J. Heat Mass Transf.* (2022) **183**:122111.
[14] Yang, L., Li, Y., Wu, S., Chen, P., Wu, H., Su, J., Wang, H., Liu, J., Yan, C. and Shi, Y. Tailorable and predictable mechanical responses of additive manufactured TPMS lattices with graded structures. *Mater. Sci. Eng. A* (2022) **843**:143109.
[15] Novak, N., Borovinšek, M., Al-Ketan, O., Ren, Z. and Vesenjak, M. Impact and blast resistance of uniform and graded sandwich panels with TPMS cellular structures. *Compos. Struct.* (2022) **300**:116174.
[16] Lu, C., Lesmana, L. A., Chen, F. and Aziz, M. MD-TPMS: Multi-dimensional gradient minimal surface generator. *Softw. Impacts* (2023) **17**:100527.
[17] Tran, T. N. D. and Piat, R. Numerical studies of crack propagation in composites reinforced by irregular particles. *Procedia Struct. Integr.* (2024) **52**:366–375.
[18] Yan, X., Dong, S., Li, X., Zhao, Z., Dong, S., and An, L. Optimization of machining parameters for milling zirconia ceramics by polycrystalline diamond tool. *Materials* (2021) **15**:208.
[19] Hibbitt K and S. ABAQUS/CAE User's Manual, Section 19.2.2 (2002).